Encapsulation and Adsorption of Halogens into Single-Walled Carbon Nanotubes

Navaratnarajah Kuganathan [1,*] and **Sashikesh Ganeshalingam** [2]

1   Department of Materials, Imperial College London, London SW7 2AZ, UK
2   Department of Chemistry, University of Jaffna, Sir. Pon Ramanathan Road, Thirunelvely, Jaffna 40000, Sri Lanka; sashikesh@gmail.com
*   Correspondence: n.kuganathan@imperial.ac.uk

Abstract: Functionalisation of single-walled carbon nanotubes (SWNTs) with atoms and molecules has the potential to prepare charge–transfer complexes for numerous applications. Here, we used density functional theory with dispersion correction (DFT + D) to examine the encapsulation and adsorption efficacy of single-walled carbon nanotubes to trap halogens. Our calculations show that encapsulation is exoergic with respect to gas-phase atoms. The stability of atoms inside SWNTs is revealed by the charge transfer between nanotubes and halogens. Encapsulation of halogens in the form of diatomic molecules is favourable with respect to both atoms and diatomic molecules as reference states. The adsorption of halogens on the outer surfaces of SWNTs is also exothermic. In all cases, the degree of encapsulation, adsorption, and charge transfer is reflected by the electronegativity of halogens.

Keywords: halogens; carbon nanotubes; DFT; encapsulation; charge transfer

1. Introduction

Carbon nanotubes have been studied for the last three decades for their applications in nanoelectronic devices [1–4], energy storage devices [5–8], biology, and medicine [9–12]. As they exhibit good chemical, thermal, and mechanical properties, they are used as building blocks for designing supramolecular arrays. This type of design is expected to modify the structural and electronic properties of nanotubes.

A variety of atoms [13,14], molecules [15,16], one-dimensional nanocrystals [17–21], nanowires [22,23], and nanoribbons [24,25] have been encapsulated experimentally inside the SWNTs. The filling of bulk material has led to the formation of the one-dimensional nanocrystal, which is different from the bulk structure [26,27]. For example, bulk zinc blende HgTe formed a three-coordinated tubular structure inside SWNT [28]. The outer surface of the nanotubes has been extensively studied theoretically for the adsorption of a variety of molecules [29–32]. Such adsorption studies have been recognised for sensor applications.

Carbon nanotubes and graphene have been effectively considered for the removal of surfactants [33–35]. Surfactants should be removed before they enter the environment as they can cause skin irritation [36]. Many experimental studies are available in the literature addressing the functionalisation of carbon surfaces to adsorb surfactants [37–39]. Zelikman et al. [40] used molecular simulations to investigate the interactions between SWNTs and surfactants. Enhancement in the binding energy was noted with the adsorption of a benzoic ring with the graphitic surface.

Halogens are also candidate species that should be considered for the encapsulation or adsorption with nanotubes as they are toxic to humans at their exceeded level. Molecular bromine and iodine are important radioactive fission products that are released from nuclear plants. In a previous simulation study [41], the interaction of single F and Cl atoms has been studied. In a combined experimental and theoretical study [42], adsorption of ICl,

Br$_2$, IBr, and I$_2$ molecules was considered. However, there are no studies available in the literature that focus on halogens interacting with carbon nanotubes.

In this study, we used spin-polarized density functional theory together with dispersion correction to study the encapsulation and adsorption of halogens (of Cl, Br, and I) in the form of atoms and molecules the three different armchair SWNTs [(8,8), (9,9) and (10,10)]. Dispersion correction is important for atoms or molecules to interact noncovalently with nanotubes. The current simulation method enabled us to calculate encapsulation or adsorption energies, the charge transfer between halogens and nanotubes, and electronic structures of encapsulated or adsorbed composites.

2. Computational Methods

We used plane wave-based DFT simulations, as implemented in the Vienna Ab initio simulation package (VASP) code [43]. The exchange-correlation term was included in the form of generalised gradient approximation (GGA) described by Perdew, Burke, and Ernzerhof (PBE) [44]. The valence electronic configurations for C, Cl, Br, and I were $2s^2 2p^2$, $3s^2 3p^5$, $4s^2 4p^5$, and $6s^2 6p^5$, respectively. A plane-wave basis set with a cut-off of 500 eV and the projected augmented wave (PAW) potentials [45] were used. For the pristine tubes and atom-encapsulated or -adsorbed tubes, a $1 \times 1 \times 4$ Monkhorst-Pack [46] k-point mesh was used. Structure optimisations were performed using a conjugate gradient algorithm [47], together with Hellman–Feynman theorem including Pulay corrections. Forces on the atoms were smaller than 0.01 eV/Å in all relaxed configurations. Dispersive attractive interactions were modelled using a semi-empirical pair-wise force field, as implemented in the VASP code [48].

Periodic boundary conditions were applied to all three nanotubes along the c axis, and a minimum lateral separation of 30 Å between adjacent structures in the other two directions was maintained. Encapsulation energy was calculated using the following Equation (1):

$$E_{enc} = E\,(X@SWNT) - E\,(SWNT) - E\,(X \text{ or } \tfrac{1}{2}\,X_2) \tag{1}$$

where E (X@SWNT) is the total energy of a halogen atom (X = Cl, Br and I) encapsulated within an SWNT; E (SWNT) and E (X or $\frac{1}{2}$ X$_2$) are the total energies of an SWNT and an isolated gas-phase halogen atom in the form of atomic or molecular state. A similar equation was also used for the calculation of adsorption energy. Bader charge analysis [49] was carried out to determine the charge transfer between tubes and halogen atoms. The density-of-states (DOS) plots were used to calculate the electronic structures of pristine SWNTs and halogen-encapsulated or -adsorbed SWNT composites.

Three different nanotubes [(8,8), (9,9), and (10,10)] were selected. Seven unit cells were extended along the tube axis to make a supercell. Table 1 lists the number of carbon atoms in each nanotube supercell and their diameters.

Table 1. Diameters and number of carbon atoms in the supercells of (8,8), (9,9), and (10,10) SWNTs.

Type	Diameter (Å)	Number of Carbon Atoms in the Super Cell
(8,8)	10.86	224
(9,9)	12.21	252
(10,10)	13.57	280

The quality of the PAW potentials for C, Cl, Br, and I used in this study was reported in our previous simulation studies [50,51].

3. Results and Discussion

3.1. Encapsulation of Halogen Atoms within SWNTs

First, we considered the encapsulation of halogen atoms within SWNTs. Relaxed structures of Cl encapsulated within (8,8), (9,9), and (10,10) SWNTs and corresponding charge density plots are shown in Figure 1. Relaxed structures of Br and I atoms encapsulated within SWNTs are similar to those presented in Figure 1 and are provided in the supplementary information (ESI, Figures S1 and S2). In all cases, halogen atoms are closer to the centre of the nanotubes.
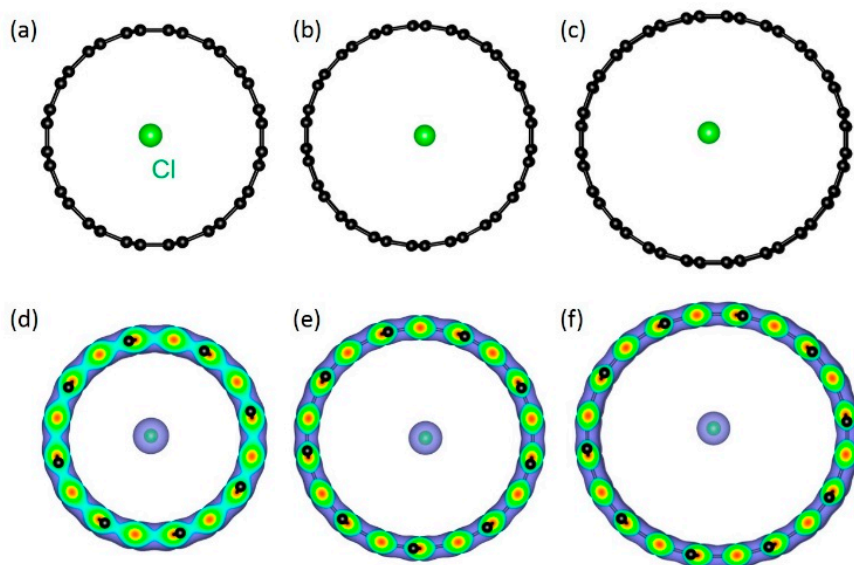

Figure 1. Relaxed structures of (**a**) Cl@(8,8), (**b**) Cl@(9,9), and (**c**) Cl@(10,10). Corresponding charge density plots (**d–f**) are also shown.

The stability of single halogen atoms was examined by calculating encapsulation energies. In Table 2, we provide encapsulation energies calculated with respect to gaseous halogen atoms and diatomic molecules and Bader charges on encapsulated halogen atoms. Encapsulation energies calculated with respect to gaseous atoms are negative, meaning that they are stable inside the SWNTs. However, encapsulation energies are positive in all cases with respect to dimers as references. This is because of the additional endothermic energy required to break dimers to form gaseous atoms. The degree of encapsulation decreases from Cl to I with any of the three SWNTs. This is clearly due to the fact that the electronegativity order of halogen is Cl > Br > I. Electronegativity values of Cl, Br, and I are 3.16, 2.96, and 2.66, respectively [52]. When the size of the nanotube increases, the encapsulation energy of a particular halogen decreases as expected. For example, encapsulation energies of Cl in (8,8), (9,9), and (10,10) tubes are −1.15 eV, −1.00 eV, and −0.92 eV, respectively. The importance of inclusion of dispersion is indicated by the higher values of encapsulation energies than those calculated without dispersion. In all cases, a small amount of charge is transferred from SWNTs to halogen. The amount of charge is observed to be dependent on the electronegativity of halogen. The charge transfer decreases when the diameter of SWNTs increases as the distance between the halogen and the tube wall increases.

Table 2. Encapsulation energies and Bader charges on halogen atoms. Numbers reported in parentheses are values calculated without dispersion.

Structures	Encapsulation Energy (eV)		Bader Charge |e|
	X (Cl or Br or I)	$\frac{1}{2}$ X$_2$ (Cl or Br or I)	
Cl@(8,8)	−1.15 (−1.05)	0.35 (0.45)	−0.59 (−0.59)
Br@(8,8)	−0.99 (−0.84)	0.27 (0.42)	−0.55 (−0.50)
I@(8,8)	−0.84 (−0.62)	0.50 (0.50)	−0.50 (−0.45)
Cl@(9,9)	−1.00 (−0.94)	0.50 (0.56)	−0.54 (−0.54)
Br@(9,9)	−0.81 (−0.72)	0.45 (0.54)	−0.50 (−0.50)
I@(9,9)	−0.64 (−0.51)	0.48 (0.61)	−0.46 (−0.45)
Cl@(10,10)	−0.92 (−0.87)	0.58 (0.63)	−0.51 (−0.51)
Br@(10,10)	−0.72 (−0.66)	0.54 (0.60)	−0.47 (−0.47)
I@(10,10)	−0.54 (−0.45)	0.58 (0.67)	−0.43 (−0.43)

The calculated density of plots for (8,8) and (9,9) tubes are shown in Figure 2. Both tubes exhibit metallic character in agreement with the fact that armchair tubes (*n,n*) are metallic.
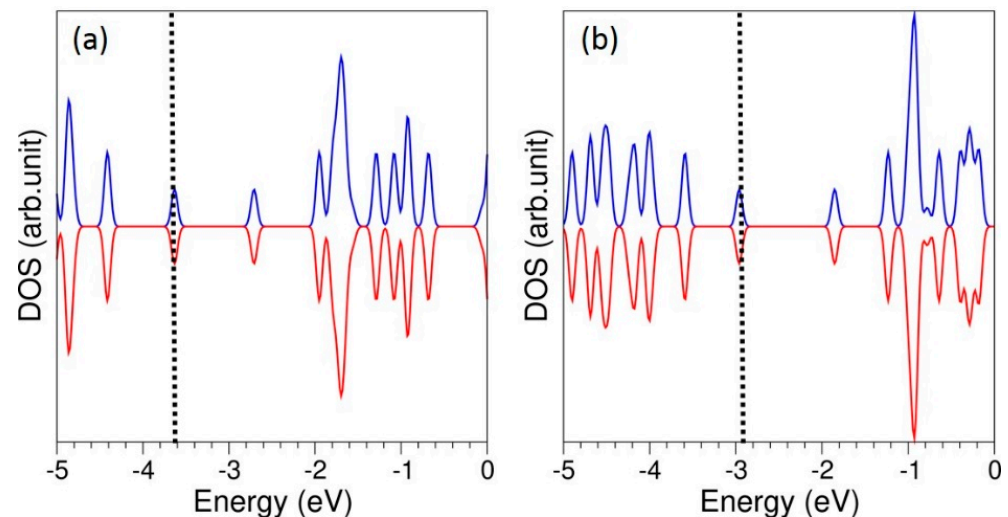

Figure 2. DOS plots calculated for (**a**) (8,8) and (**b**) (9,9) tubes.

Figure 3 shows the calculated total DOS plots of Cl, Br, and I encapsulated within (9,9) tube and atomic DOS plot of Cl, Br, and I. SWNTs still exhibit metallic character.

3.2. Adsorption of Halogen Atoms on the Surfaces of SWNTs

Next, halogen atoms were allowed to adsorb on the surfaces of SWNTs. Three possible sites (H, 66, and C) were considered (see Figure 4). In configuration H, the atom is positioned above the centre of the hexagonal ring. Atoms are positioned above the centre of the bond connecting adjacent six-membered rings and the three coordinated carbon in 66 and C configurations.
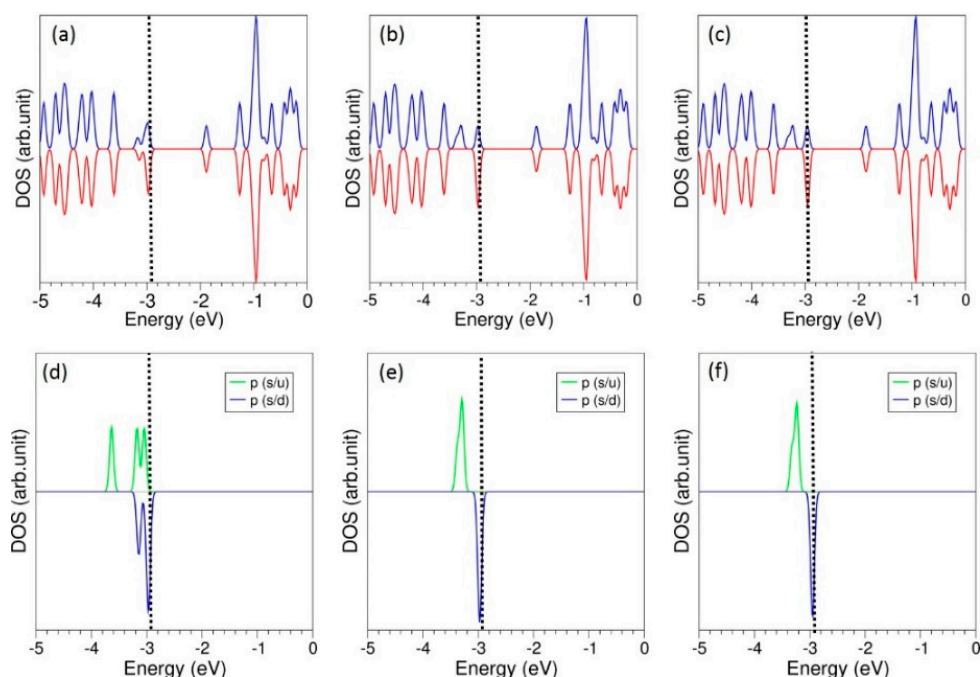
Figure 3. Calculated total DOS plots for (**a**) Cl@(9,9), (**b**) Br@(9,9), and (**c**) I@(9,9). Corresponding atomic DOS plots for Cl, Br, and I (**d**–**f**) are also shown.
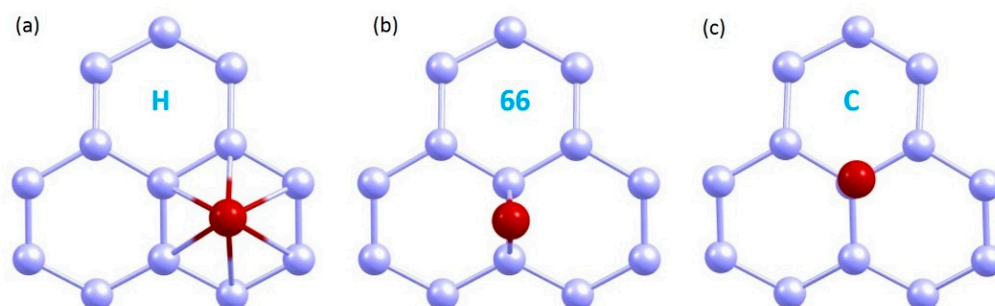

Figure 4. Starting configurations considered for the adsorption of halogens on the SWNT: (**a**) H, (**b**) 66, and (**c**) C.

All three configurations were fully relaxed for the (8,8) tube. Relative energies are shown in Table 3. The lowest energy structure is calculated to be the C configuration.

Table 3. Relative energies of three different outer surface configurations of a (8,8) tube.

Configuration	Relative Energy (eV)
C	0.00
66	0.02
H	0.05

Next, we considered the adsorption of halogen atoms on the surfaces of all three SWNTs. The relaxed structures of halogens adsorbed on the (9,9) tube are shown in Figure 5. Adsorption is exoergic with respect to gas-phase atoms (refer to Table 4), meaning that atoms are stable on the surface of SWNTs. Stronger adsorption is calculated with dispersion correction in all cases. The diameter of the nanotube does not significantly change the adsorption energies. Negative Bader charges on the halogen atoms indicate that there is a charge transfer from tubes to halogen atoms. The electronegativity of halogen

reflects in the amount of charge transferred. This is further confirmed by the C–X distances, as listed in Table 4.
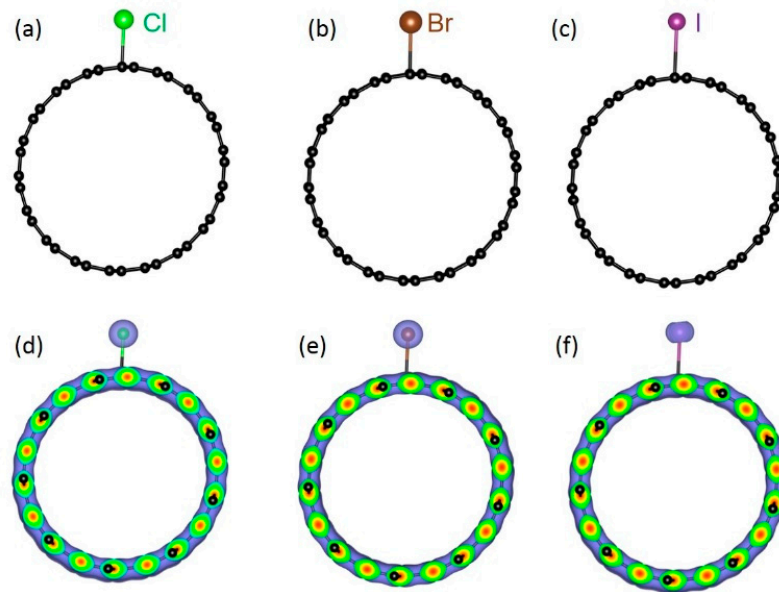

Figure 5. Relaxed structures of (**a**) Cl, (**b**) Br, and (**c**) I adsorbed on the surface of the (9,9) tube. Corresponding charge density plots (**d**–**f**) are also shown.

Table 4. Adsorption energies and Bader charges on halogen atoms. Numbers reported in parentheses are values calculated without dispersion.

Structures	Adsorption Energy (eV)		Bader Charge |e|	C-X (Å)
	X (Cl or Br or I)	$\frac{1}{2}$ X$_2$ (Cl or Br or I)		
Cl_(8,8)	−1.01 (−0.88)	0.49 (0.62)	−0.54 (−0.54)	2.67 (2.70)
Br_(8,8)	−0.79 (−0.61)	0.47 (0.65)	−0.45 (−0.47)	3.02 (3.21)
I_(8,8)	−0.52 (−0.36)	0.60 (0.76)	−0.39 (−0.39)	3.41 (3.50)
Cl_(9,9)	−1.01 (−0.89)	0.49 (0.61)	−0.50 (−0.50)	2.66 (2.69)
Br_(9,9)	−0.77 (−0.63)	0.49 (0.63)	−0.44 (−0.44)	3.08 (3.15)
I_(9,9)	−0.54 (−0.38)	0.58 (0.74)	−0.36 (−0.36)	3.37 (3.21)
Cl_(10,10)	−1.00 (−0.88)	0.50 (0.62)	−0.50 (−0.50)	2.91 (2.78)
Br_(10,10)	−0.75 (−0.61)	0.51 (0.65)	−0.44 (−0.44)	3.12 (3.26)
I_(10,10)	−0.53 (−0.38)	0.59 (0.74)	−0.37 (−0.37)	3.51 (3.64)

Figure 6 shows the total and atomic DOS plots calculated for Cl, Br, and I atoms adsorbed on the surface of (9,9) tube. All three resultant complexes exhibit metallic character, as calculated for pristine nanotubes. The Fermi energy levels are partly occupied by the p-state halogen atoms (see Figure 6).
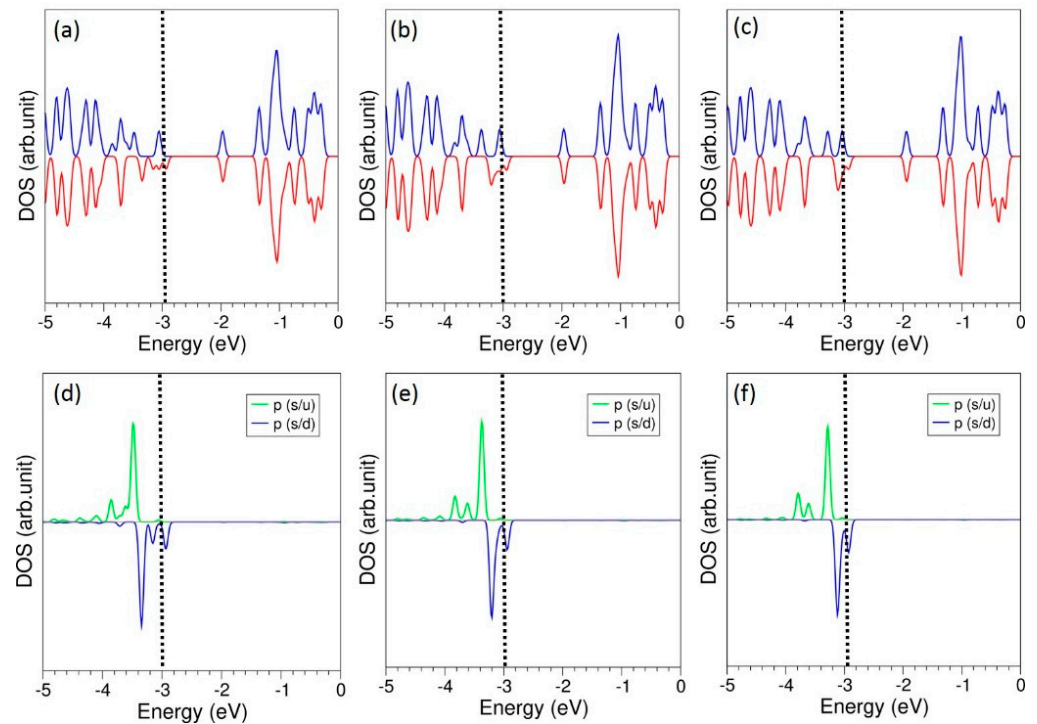
Figure 6. Calculated total DOS plots for (**a**) Cl@(9,9), (**b**) Br@(9,9), and (**c**) I@(9,9). Corresponding atomic DOS plots for Cl, Br, and I (**d–f**) are also shown.

3.3. Encapsulation of Molecular Halogens inside SWNTs

Here, we examine the formation of halogen dimers inside SWNTs. Two different possible configurations (along the tube axis and perpendicular to the tube axis) were considered. Relaxed structures of Cl_2, Br_2, and I_2 molecules encapsulated within SWNTs are shown in Figure 7. Table 5 reports the encapsulation energies, Bader charges on halogen molecules, and intermolecular distances of halogens.
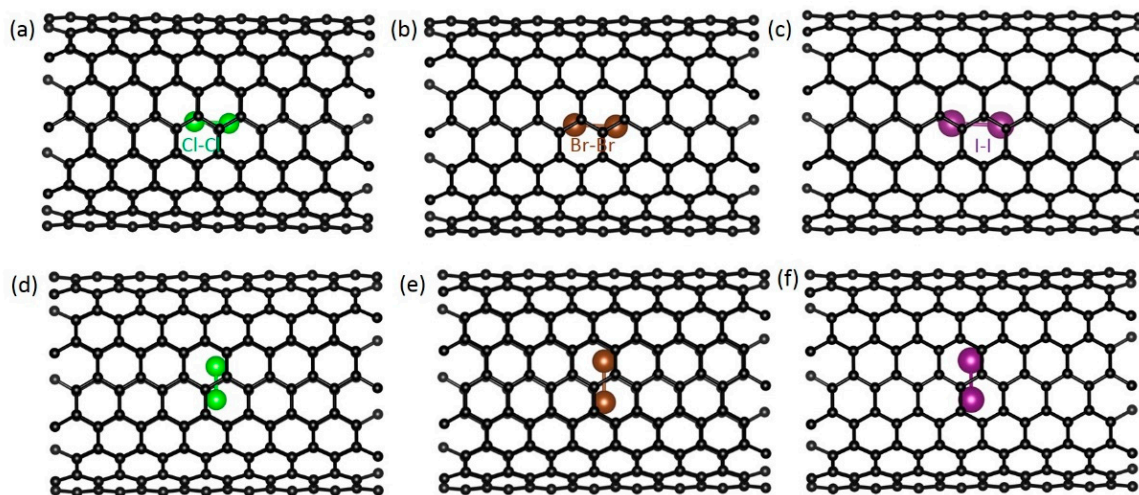

Figure 7. Relaxed structures of (**a**) Cl_2, (**b**) Br_2, and (**c**) I_2 molecules configured along the (9,9) tube axis and (**d–f**) corresponding molecules positioning perpendicular to the tube axis.

Table 5. Encapsulation energies, Bader charges on halogen molecules, and intermolecular distances of halogens. Numbers reported in parentheses are values calculated without dispersion: A, along the axis; C, perpendicular to the tube axis.

Structures	Encapsulation Energy (eV)/X Atom		Bader Charge $\lvert e \rvert$	X-X (Å)
	X (Cl or Br)	X_2 (Cl or Br)		
Cl_2@(8,8)_A	−1.62 (−1.52)	−0.11 (−0.005)	−0.07/+0.05 (−0.07/+0.04)	2.01 (2.01)
Cl_2@(8,8)_C	−1.60 (−1.52)	−0.15 (−0.015)	−0.03/−0.02 (−0.02/−0.01)	2.02 (2.01)
Br_2@(8,8)_A	−1.43 (−1.28)	−0.18 (−0.025)	−0.13/−0.05 (−0.11/−0.04)	2.38 (2.36)
Br_2@(8,8)_C	−1.48 (−1.29)	−0.23 (−0.03)	−0.09/−0.09 (−0.09/−0.09)	2.41 (2.40)
I_2@(8,8)_A	−1.32 (−1.19)	−0.19 (−0.05)	−0.08/−0.07 (−0.08/−0.06)	2.73 (2.72)
I_2@(8,8)_C	−1.36 (−1.21)	−0.21 (−0.06)	−0.07/−0.06 (−0.05/−0.04)	2.72 (2.71)
Cl_2@(9,9)_A	−1.57 (−1.51)	−0.06 (0.00)	−0.05/+0.04 (−0.04/+0.05)	1.99 (2.00)
Cl_2@(9,9)_C	−1.59 (−1.52)	−0.08 (−0.005)	−0.04/+0.03 (−0.04/+0.03)	2.00 (2.00)
Br_2@(9,9)_A	−1.35 (−1.26)	−0.10 (−0.01)	−0.10/−0.03 (−0.10/−0.03)	2.36 (2.36)
Br_2@(9,9)_C	−1.39 (−1.27)	−0.13 (−0.02)	−0.09/−0.04 (−0.10/−0.04)	2.37 (2.36)
I_2@(9,9)_A	−1.28 (−1.10)	−0.12 (−0.03)	−0.06/−0.05 (−0.04/−0.03)	2.74 (2.73)
I_2@(9,9)_C	−1.25 (−1.16)	−0.13 (−0.04)	−0.05/−0.03 (−0.04/−0.02)	2.71 (2.70)
Cl_2@(10,10)_A	−1.56 (−1.51)	−0.05 (0.00)	−0.04/+0.03 (−0.03/−0.04)	1.99 (2.00)
Cl_2@(10,10)_C	−1.56 (−1.51)	−0.05 (0.00)	−0.01/+0.01 (−0.01/−0.01)	2.00 (2.00)
Br_2@(10,10)_A	−1.32 (−1.26)	−0.06 (−0.005)	−0.07/−0.01 (−0.02/−0.08)	2.34 (2.34)
Br_2@(10,10)_C	−1.33 (−1.26)	−0.08 (−0.005)	−0.05/−0.05 (−0.05/−0.05)	2.34 (2.34)
I_2@(10,10)_A	−1.20 (−1.08)	−0.10 (−0.02)	−0.05/−0.03 (−0.03/−0.02)	2.70 (2.69)
I_2@(10,10)_C	−1.22 (−1.10)	−0.11 (−0.03)	−0.04/−0.02 (−0.03/−0.02)	2.68 (269)

Encapsulation energies are negative with respect to both atom and molecule as reference states indicate that the formation of dimers is possible inside SWNTs. The inclusion of dispersion strengthens the encapsulation. The electronegativity of halogens also influences encapsulation. Stronger encapsulation is reflected by higher electronegative halogen. Bader charge analysis shows that dimers are polarised in most cases, and the total charge on the molecules is very small. There is only a small energy difference between the two configurations (along the axis and perpendicular to the axis). Isolated dimer distances of Cl_2, Br_2, and I_2 in this study are 1.99 Å, 2.32 Å, and 2.69 Å, respectively. Encapsulation has a small effect on dimer distances. Elongation in the dimer distances increases with the size of the molecules.

3.4. Adsorption of Molecular Halogens on the Surfaces of SWNTs

Finally, we considered the stability of dimers adsorbed on the surfaces of SWNTs. Figure 8 shows the relaxed structures of Cl_2, Br_2, and I_2 adsorbed on the (9,9) tube. Table 6 lists the adsorption energies, Bader charges on the molecules, and dimer distances.
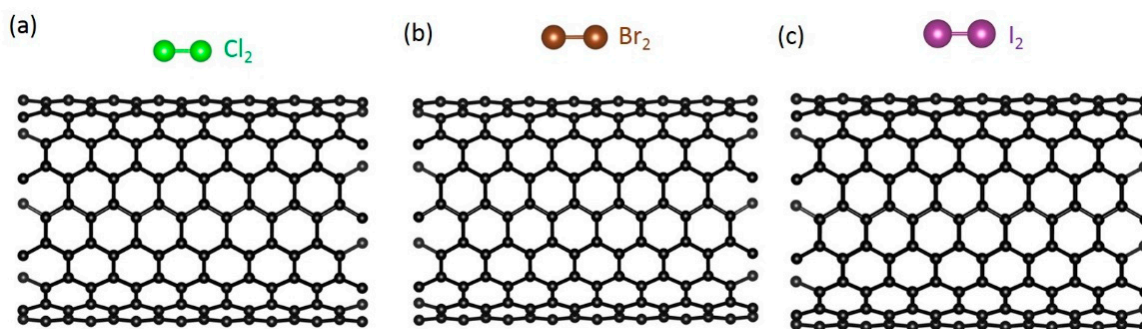

Figure 8. Relaxed structures of (**a**) Cl_2, (**b**) Br_2, and (**c**) I_2 adsorbed on the (9,9) tube.

Table 6. Adsorption energies, Bader charges on halogen molecules, and intermolecular distances of halogens. Numbers reported in parentheses are values calculated without dispersion.

Structures	Adsorption Energy (eV)/X Atom		Bader Charge |e|	X-X (Å)
	X (Cl or Br or I)	X$_2$ (Cl or Br or I)		
Cl$_2$_(9,9)	−1.59 (−1.50)	−0.08 (−0.01)	−0.01/+0.02 (−0.01/+0.03)	1.99 (2.00)
Br$_2$_(9,9)	−1.36 (−1.27)	−0.06 (−0.02)	−0.04/+0.01 (−0.03/+0.01)	2.32 (2.01)
I$_2$_(9,9)	−1.23 (−1.12)	−0.03 (−0.01)	−0.06/+0.03 (−0.05/+0.02)	2.74 (2.73)

In all cases, adsorption is exothermic with respect to gas-phase atoms and dimers. The highest adsorption energy is calculated for the Cl due to its highest electronegativity. Bader charge analysis shows that dimers are polarised, and there is a negligible charge transfer between tubes and molecules. Dimer distances in the relaxed configurations are closer to the distances calculated in the isolated dimers.

4. Conclusions

In this study, we used DFT simulation, together with dispersion, to examine the encapsulation and adsorption of gas-phase halogen atoms and dimers. Strong encapsulation energies were calculated for all three halogen atoms with respect to their gas-phase atoms. A significant charge transfer from nanotubes to halogens was noted in all cases. Diatomic molecules were also stable inside SWNTs with respect to both atoms and diatomic molecules as reference states. Exothermic adsorption energies were calculated for all three halogens, meaning that they can be trapped via the outer surfaces of SWNTs. Electronegativity of halogens determines the nature of encapsulation or adsorption and the amount of charge transferred between SWNTs and halogens.

References

1. Khanna, V.K. Carbon Nanotube-Based Nanoelectronics. In *Integrated Nanoelectronics: Nanoscale CMOS, Post-CMOS and Allied Nanotechnologies*; Springer: New Delhi, India, 2016; pp. 285–302.
2. Liebau, M.; Graham, A.P.; Duesberg, G.S.; Unger, E.; Seidel, R.; Kreupl, F. Nanoelectronics Based on Carbon Nanotubes: Technological Challenges and Recent Developments. *Fuller. Nanotub. Carbon Nanostructures* **2005**, *13*, 255–258. [CrossRef]
3. Cao, Q.; Han, S.-J. Nanoelectronics Based on Single-Walled Carbon Nanotubes. In *Nanomaterials, Polymers, and Devices*; John Wiley & Sons Inc.: Hoboken, NJ, USA, 2015; pp. 501–522.
4. Che, Y.; Chen, H.; Gui, H.; Liu, J.; Liu, B.; Zhou, C. Review of carbon nanotube nanoelectronics and macroelectronics. *Semicond. Sci. Technol.* **2014**, *29*, 073001. [CrossRef]
5. Sun, L.; Wang, X.; Wang, Y.; Zhang, Q. Roles of carbon nanotubes in novel energy storage devices. *Carbon* **2017**, *122*, 462–474. [CrossRef]
6. Cao, Z.; Wei, B. A perspective: Carbon nanotube macro-films for energy storage. *Energy Environ. Sci.* **2013**, *6*, 3183–3201. [CrossRef]

7. Chen, Z.; Lv, T.; Yao, Y.; Li, H.; Li, N.; Yang, Y.; Liu, K.; Qian, G.; Wang, X.; Chen, T. Three-dimensional seamless graphene/carbon nanotube hybrids for multifunctional energy storage. *J. Mater. Chem. A* **2019**, *7*, 24792–24799. [CrossRef]

8. Zhan, H.; Zhang, G.; Bell, J.M.; Tan, V.B.C.; Gu, Y. High density mechanical energy storage with carbon nanothread bundle. *Nat. Commun.* **2020**, *11*, 1905. [CrossRef] [PubMed]

9. Wang, X.; Liu, Z. Carbon nanotubes in biology and medicine: An overview. *Chin. Sci. Bull.* **2012**, *57*, 167–180. [CrossRef]

10. Yang, W.; Thordarson, P.; Gooding, J.J.; Ringer, S.P.; Braet, F. Carbon nanotubes for biological and biomedical applications. *Nanotechnology* **2007**, *18*, 412001. [CrossRef]

11. Liu, Z.; Tabakman, S.; Welsher, K.; Dai, H. Carbon Nanotubes in Biology and Medicine: In vitro and in vivo Detection, Imaging and Drug Delivery. *Nano. Res.* **2009**, *2*, 85–120. [CrossRef]

12. Anzar, N.; Hasan, R.; Tyagi, M.; Yadav, N.; Narang, J. Carbon nanotube—A review on Synthesis, Properties and plethora of applications in the field of biomedical science. *Sens. Int.* **2020**, *1*, 100003. [CrossRef]

13. Fan, J.; Chamberlain, T.W.; Wang, Y.; Yang, S.; Blake, A.J.; Schröder, M.; Khlobystov, A.N. Encapsulation of transition metal atoms into carbon nanotubes: A supramolecular approach. *Chem. Commun.* **2011**, *47*, 5696–5698. [CrossRef]

14. Huang, X.; Yu, H.; Tan, H.; Zhu, J.; Zhang, W.; Wang, C.; Zhang, J.; Wang, Y.; Lv, Y.; Zeng, Z.; et al. Carbon Nanotube-Encapsulated Noble Metal Nanoparticle Hybrid as a Cathode Material for Li-Oxygen Batteries. *Adv. Funct. Mater.* **2014**, *24*, 6516–6523. [CrossRef]

15. del Carmen Giménez-López, M.; Moro, F.; La Torre, A.; Gómez-García, C.J.; Brown, P.D.; van Slageren, J.; Khlobystov, A.N. Encapsulation of single-molecule magnets in carbon nanotubes. *Nat. Commun.* **2011**, *2*, 407. [CrossRef]

16. Dappe, Y. Encapsulation of organic molecules in carbon nanotubes: Role of the van der Waals interactions. *J. Phys. D* **2014**, *47*, 083001. [CrossRef]

17. Kuganathan, N.; Green, J.C. Mercury telluride crystals encapsulated within single walled carbon nanotubes: A density functional study. *Int. J. Quantum Chem.* **2008**, *108*, 797–807. [CrossRef]

18. Kuganathan, N.; Chroneos, A. Encapsulation of cadmium telluride nanocrystals within single walled carbon nanotubes. *Inorg. Chim. Acta* **2019**, *488*, 246–254. [CrossRef]

19. Calatayud, D.G.; Ge, H.; Kuganathan, N.; Mirabello, V.; Jacobs, R.M.J.; Rees, N.H.; Stoppiello, C.T.; Khlobystov, A.N.; Tyrrell, R.M.; Da Como, E.; et al. Encapsulation of Cadmium Selenide Nanocrystals in Biocompatible Nanotubes: DFT Calculations, X-ray Diffraction Investigations, and Confocal Fluorescence Imaging. *Chem. Open* **2018**, *7*, 144–158. [CrossRef] [PubMed]

20. Sloan, J.; Novotny, M.C.; Bailey, S.R.; Brown, G.; Xu, C.; Williams, V.C.; Friedrichs, S.; Flahaut, E.; Callender, R.L.; York, A.P.E.; et al. Two layer 4:4 co-ordinated KI crystals grown within single walled carbon nanotubes. *Chem. Phys. Lett.* **2000**, *329*, 61–65. [CrossRef]

21. Thamavaranukup, N.; Höppe, H.A.; Ruiz-Gonzalez, L.; Costa, P.M.F.J.; Sloan, J.; Kirkland, A.; Green, M.L. Single-walled carbon nanotubes filled with M OH (M = K, Cs) and then washed and refilled with clusters and molecules. *Chem. Commun.* **2004**, *15*, 1686–1687. [CrossRef]

22. Morelos-Gómez, A.; López-Urías, F.; Muñoz-Sandoval, E.; Dennis, C.L.; Shull, R.D.; Terrones, H.; Terrones, M. Controlling high coercivities of ferromagnetic nanowires encapsulated in carbon nanotubes. *J. Mater. Chem.* **2010**, *20*, 5906–5914. [CrossRef]

23. Li, Y.; Bai, H.; Li, L.; Huang, Y. Stabilities and electronic properties of nanowires made of single atomic sulfur chains encapsulated in zigzag carbon nanotubes. *Nanotechnology* **2018**, *29*, 415703. [CrossRef] [PubMed]

24. Chuvilin, A.; Bichoutskaia, E.; Giménez-López, M.; Chamberlain, T.; Rance, G.; Kuganathan, N.; Biskupek, J.; Kaiser, U.; Khlobystov, A.N. Self-assembly of a sulphur-terminated graphene nanoribbon within a single-walled carbon nanotube. *Nat. Mater.* **2011**, *10*, 687–692. [CrossRef]

25. Furuhashi, F.; Shintani, K. Morphology of a graphene nanoribbon encapsulated in a carbon nanotube. *AIP Adv.* **2013**, *3*, 092103. [CrossRef]

26. Sloan, J.; Kirkland, A.I.; Hutchison, J.L.; Green, M.L.H. Integral atomic layer architectures of 1D crystals inserted into single walled carbon nanotubes. *Chem. Commun.* **2002**, *13*, 1319–1332. [CrossRef]

27. Sloan, J.; Kirkland, A.I.; Hutchison, J.L.; Green, M.L.H. Structural Characterization of Atomically Regulated Nanocrystals Formed within Single-Walled Carbon Nanotubes Using Electron Microscopy. *Acc. Chem. Res.* **2002**, *35*, 1054–1062. [CrossRef] [PubMed]

28. Carter, R.; Sloan, J.; Kirkland, A.I.; Meyer, R.R.; Lindan, P.J.D.; Lin, G.; Green, M.L.; Vlandas, A.; Hutchison, J.L.; Harding, J. Correlation of Structural and Electronic Properties in a New Low-Dimensional Form of Mercury Telluride. *Phys. Rev. Lett.* **2006**, *96*, 215501. [CrossRef]

29. Jia, X.; An, L.; Chen, T. Adsorption of nitrogen oxides on Al-doped carbon nanotubes: The first principles study. *Adsorption* **2020**, *26*, 587–595. [CrossRef]

30. Li, Y.; Hodak, M.; Lu, W.; Bernholc, J. Mechanisms of NH_3 and NO_2 detection in carbon-nanotube-based sensors: An ab initio investigation. *Carbon* **2016**, *101*, 177–183. [CrossRef]

31. Wang, Y.; Yeow, J.T.W. A Review of Carbon Nanotubes-Based Gas Sensors. *J. Sens.* **2009**, *2009*, 493904. [CrossRef]

32. Xie, C.; Sun, Y.; Zhu, B.; Song, W.; Xu, M. Adsorption mechanism of NH_3, NO, and O_2 molecules over the Fe_xO_y/AC catalyst surface: A DFT-D3 study. *New J. Chem.* **2021**, *45*, 3169–3180. [CrossRef]

33. Tkalya, E.E.; Ghislandi, M.; de With, G.; Koning, C.E. The use of surfactants for dispersing carbon nanotubes and graphene to make conductive nanocomposites. *Curr. Opin. Colloid Interface Sci.* **2012**, *17*, 225–232. [CrossRef]

34. Fatemi, S.M.; Foroutan, M. Recent developments concerning the dispersion of carbon nanotubes in surfactant/polymer systems by MD simulation. *J. Nanostructure Chem.* **2016**, *6*, 29–40. [CrossRef]

35. Borode, A.O.; Ahmed, N.A.; Olubambi, P.A. Surfactant-aided dispersion of carbon nanomaterials in aqueous solution. *Phys. Fluids* **2019**, *31*, 071301. [CrossRef]

36. Wilhelm, K.-P.; Freitag, G.; Wolff, H.H. Surfactant-induced skin irritation and skin repair: Evaluation of the acute human irritation model by noninvasive techniques. *J. Am. Acad. Dermatol.* **1994**, *30*, 944–949. [CrossRef]

37. Di Crescenzo, A.; Di Profio, P.; Siani, G.; Zappacosta, R.; Fontana, A. Optimizing the Interactions of Surfactants with Graphitic Surfaces and Clathrate Hydrates. *Langmuir* **2016**, *32*, 6559–6570. [CrossRef] [PubMed]

38. Rausch, J.; Zhuang, R.-C.; Mäder, E. Surfactant assisted dispersion of functionalized multi-walled carbon nanotubes in aqueous media. *Compos. Part A Appl. Sci. Manuf.* **2010**, *41*, 1038–1046. [CrossRef]

39. Le, V.T.; Ngo, C.L.; Le, Q.T.; Ngo, T.T.; Nguyen, D.N.; Vu, M.T. Surface modification and functionalization of carbon nanotube with some organic compounds. *Adv. Nat. Sci. Nanosci. Nanotechnol.* **2013**, *4*, 035017. [CrossRef]

40. Zelikman, E.; Alperstein, D.; Mechrez, G.; Suckeveriene, R.; Narkis, M. Study of interactions between single-wall carbon nanotubes and surfactant using molecular simulations. *Polym. Bull.* **2013**, *70*, 1195–1204. [CrossRef]

41. Pan, H.; Feng, Y.P.; Lin, J.Y. Ab initiostudy of F- and Cl-functionalized single wall carbon nanotubes. *J. Phys. Condens. Matter* **2006**, *18*, 5175–5184. [CrossRef]

42. Ghosh, S.; Yamijala, S.R.K.C.S.; Pati, S.K.; Rao, C.N.R. The interaction of halogen molecules with SWNTs and graphene. *RSC Adv.* **2012**, *2*, 1181–1188. [CrossRef]

43. Kresse, G.; Furthmüller, J. Efficient iterative schemes for ab initio total-energy calculations using a plane-wave basis set. *Phys. Rev. B* **1996**, *54*, 11169–11186. [CrossRef] [PubMed]

44. Perdew, J.P.; Burke, K.; Ernzerhof, M. Generalized Gradient Approximation Made Simple. *Phys. Rev. Lett.* **1996**, *77*, 3865–3868. [CrossRef]

45. Blöchl, P.E. Projector augmented-wave method. *Phys. Rev. B* **1994**, *50*, 17953–17979. [CrossRef]

46. Monkhorst, H.J.; Pack, J.D. Special points for Brillouin-zone integrations. *Phys. Rev. B* **1976**, *13*, 5188–5192. [CrossRef]

47. Press, W.H.; Teukolsky, S.A.; Vetterling, W.T.; Flannery, B.P. *Numerical Recipes in C: The Art of Scientific Computing*, 2nd ed.; Cambridge University Press: Cambridge, UK, 1992.

48. Grimme, S.; Antony, J.; Ehrlich, S.; Krieg, H. A consistent and accurate ab initio parametrization of density functional dispersion correction (DFT-D) for the 94 elements H-Pu. *J. Chem. Phys.* **2010**, *132*, 154104. [CrossRef] [PubMed]

49. Henkelman, G.; Arnaldsson, A.; Jónsson, H. A fast and robust algorithm for Bader decomposition of charge density. *Comput. Mater. Sci.* **2006**, *36*, 354–360. [CrossRef]

50. Kuganathan, N.; Selvanantharajah, N.; Iyngaran, P.; Abiman, P.; Chroneos, A. Cadmium trapping by C_{60} and B-, Si-, and N-doped C_{60}. *J. Appl. Phys.* **2019**, *125*, 054302. [CrossRef]

51. Kuganathan, N.; Ghosh, P.S.; Arya, A.K.; Dey, G.K.; Grimes, R.W. Energetics of halogen impurities in thorium dioxide. *J. Nucl. Mater.* **2017**, *495*, 192–201. [CrossRef]

52. Lide, D.R. *CRC Handbook of Chemistry and Physics*, 86th ed.; CRC: Boca Raton, FL, USA, 2005.